Materials & Design, DOI: 10.1016/j.matdes.2016.05.021 (2016)

Influence of κ-carbide interface structure on the formability of lightweight steels

W.J. Lu[1] and R.S. Qin[1, 2 *]

1. Department of Materials, Imperial College London, Exhibition Road, London SW7 2AZ, UK

2. Department of Engineering & Innovation, The Open University, Milton Keynes MK7 6AA, UK

Abstract

κ-carbide (κ) in high aluminium (Al) steels is grown from austenite (γ) via γ→γ+κ or γ→α+κ (α represents ferrite), and is a lamellar structure. This work demonstrates that the formability of high Al lightweight steels is affected by the lattice misfit and interface shape between κ and matrix. The cold workability can be improved by either to change the steel chemical constitution or to implement an electro-thermo-mechanical process. For ferrite-matrix-based high Al steel, electric-current promotes the spheroidization and refinement of κ structure and reduces volume fraction of κ phase. This retards the crack nucleation and propagation, and hence improves the materials formability. The observation is caused by a direct effect of electric-current rather than side effects.

Keywords: cracking, microstructure, κ-carbide, lightweight steel

*Corresponding authors. Tel.: +44 (0)1908 652999. *E-mail addresses:* qin2020@gmail.com (R.S. Qin).

1. Introduction

Adding aluminium (Al) to steel reduces its mass density. Lightweight steel is desirable in manufacturing of fuel-economy and emission-reduction transportation components [1]. The challenge in fabrication of high Al steel includes clogging in continuous casting and cracking in cold working. The former is still outstanding due to mold flux problem. Some progress has been made in solving the latter challenge [2-6]. It is noticed that a high Al steel with austenite (γ) matrix possesses better formability than that with ferrite (α) matrix [7]. Mn stabilizes γ phase [8] and affects the plastic properties by influence on the specific stacking fault energy [9]. Fe-Mn-Al-C steel with sufficient high Mn composition is able to retain γ matrix to ambient temperature. Rapid quench helps to retain γ phase when martensitic, bainitic and ferritic transformations can be avoided. κ-carbide (κ) has a formula $(Fe,Mn)_3AlC$ and is the face-centred-cubic crystal structure. κ in high Al steel is formed by spinodal decomposition or eutectoid decomposition of γ. Spinodal decomposition in high Mn high Al steel leads to $\gamma \rightarrow \gamma + L1_2$ reaction, where $L1_2$ phase forms from an ordering reaction of the solute-enriched low temperature γ phase and subsequently transforms into κ-carbide [10]. Eutectoid decomposition of γ in low Mn (typically with a Mn content up to 10 wt.%) high Al steel leads to $\gamma \rightarrow \alpha + \kappa$. This is ferritic-matrix-based (α) but may contain a fraction of γ. In addition to κ phase formed by the spinodal/eutectoid decomposition, κ precipitates may form at the austenite grain boundaries after long annealing periods [11]. The steels with high Mn low Al and high Mn no Al are found free from κ, with γ matrix and in excellent formability

[12-13]. κ-carbide appears when Al composition becomes significant in steel [8,14-15]. The eutectoid reaction in Fe-Mn-Al-C lightweight steels has been studied systematically [16]. The forming properties of Fe-Mn-Al-C lightweight steels have been reviewed comprehensively [17-18]. A lightweight steel fabricated with designed chemical-thermo-mechanical processing achieves a tensile strength >780 MPa and elongation >30% [7]. It consists of nanoscale κ-carbides and γ-matrix. The nanoscale κ-carbides provide strengthening to the steel [15].

As is well-known, Mn is heavier and more expensive than Al. Low Mn constitution however, leads to the formation of α matrix and poor formability [8]. Other cheap and light γ-stabilizing elements (e.g. carbon or silicon) may cause other engineering problems (e.g. weldability or surface problem) [19]. The aim of this work was to find out how the formability of high Al steel was affected by its microstructure and how the cold work property could be improved. The structure-property analysis of γ-matrix-based and α-matrix-based lightweight steels are presented in Section 2. The electric-current treatment of α-matrix-based lightweight steel is described in Section 3. The processing mechanisms are investigated in Section 4. Section 5 summarized the conclusions.

2. The microstructure-formability relationship

The first objective of present research was to identify the microstructure differences between γ-matrix-based and α-matrix-based high Al steels. The former is better than

the latter in term of formability. To this purpose two types of ingot with respective chemical compositions of Fe-26Mn-9Al-0.75C and Fe-34Mn-9Al-0.65C (wt.%) were prepared using induction furnace. The microstructure and Vickers hardness of both steels after various annealing processes have been characterized previously [8, 14]. This helps to the design of thermomechanical processing conditions for the present research. The as-cast ingots were reheated to 1200 ^{o}C for 4 hours, followed by hot-rolling reduction from 30 mm to 3 mm thick plates at 1100 ^{o}C and then quenched in cold water before annealed at 600 ^{o}C and 700 ^{o}C respectively for 6 hours and then quenched in cold water again.

The microstructure of steel is affected by not only its chemical constitution but also the thermomechanical processing conditions. It is possible to made γ-matrix-based steel with a chemical composition in the range of 12-35 wt.% Mn, 0-12wt.% Al and 0.5-1.3wt.% C using adequate processing conditions. A steel containing 26 wt.% Mn is considered high Mn steel. The Mn compositions in both steels are high enough to affect the specific stacking fault energy. Choosing of an annealing temperature of 700°C for Fe-26Mn-9Al-0.75C steel rather than 600 ^{o}C was to maximize its κ-α interface fraction [14]. It is impossible to generate different microstructures using two steels with identical chemical compositions and also the same thermomechanical processing conditions.

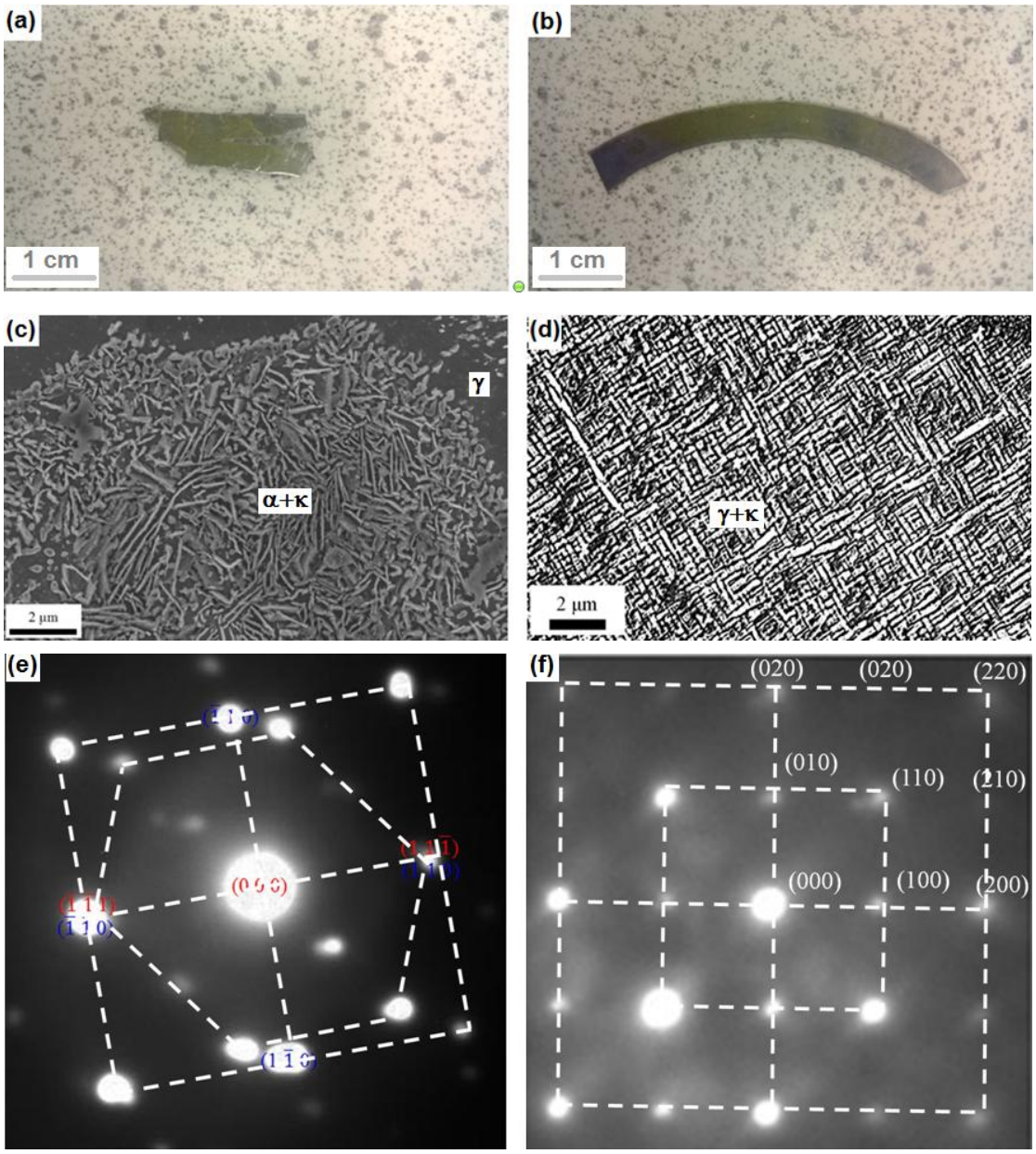


Fig. 1 Optical images for (a) Fe-26Mn-9Al-0.75C (wt.%, lower Mn) and (b) Fe-34Mn-9Al-0.65C (wt.%, higher Mn) steels after cold rolling at room temperature. SEM micrographs for (c) a lower Mn and (d) a higher Mn steels. TEM selected area diffraction patterns (SADP) for (e) a lower Mn sample and (f) a higher Mn sample.

The samples cut from each ingot were cold rolled to 70% reduction using an automatic rolling machine in order to examine their cold formability. Microstructure

analyses were performed at room temperature using optical microscopy (OM), LEO scanning electron microscopy (SEM) and JEOL 2000FX transmission electron microscopy (TEM). Samples for OM and SEM analyses were grounded, polished and etched in 2 wt.% Nital for 10 seconds. Samples for TEM analysis were mechanically polished to 30 μm thick, punched to a disk of 3 mm diameter by a copper disk cutter and then jet polished to thin foil specimens in perchloric acid (10 %) and acetic acid (90 %) mixture under 20 V at 15 ^{o}C. The electrical conductivity was measured using Microhmmeter (DO5000 series).

Fe-26Mn-9Al-0.75C samples (hereinafter to be referred as lower Mn samples) are cracked severely after cold rolling. A representative OM image for these samples is shown in Fig. 1(a). Fe-34Mn-9Al-0.65C samples (hereinafter to be referred as higher Mn samples) however, have no crack observed in their cold-rolled samples surface, as is illustrated in Fig. 1(b). Both steels have the same Al but slightly different Mn compositions. The higher Mn steel has better formability than that of the lower Mn steel. SEM analysis reveals the microstructure of the samples, as are presented in Fig. 1(c) for a lower Mn sample and Fig. 1(d) for a higher Mn samples. Both samples are with lamellar structure despite higher Mn sample demonstrates finer and more regular structure than that of lower Mn samples. TEM selected area diffraction pattern (SADP) results are presented in Fig. 1(e) for a lower Mn sample and in Fig. 1(f) for a higher Mn sample. Based on the lattice parameter calculation and crystal structure analysis, the lamellar phase in both steels is found to be κ-carbide with lattice parameter 3.75 Å.

The matrix in SADP for lower Mn sample is body-centred-cubic α phase with lattice parameter 2.92 Å. The diffraction pattern confirms the $(11\bar{1})_{\kappa} // (110)_{\alpha}$ and $[011]_{\kappa} // [001]_{\alpha}$ orientation relationships between κ-carbide and α-matrix. The matrix in higher Mn sample is face-centred-cubic γ phase with lattice parameter 3.66 Å. The orientation relationships between κ-carbide and γ-matrix are $(001)_{\kappa}// (001)_{\gamma}$ and $[001]_{\kappa}$ $//[001]_{\gamma}$. The lattice parameters for those phases are 3.61 Å for γ, 2.86 Å for α and 3.78 Å for κ-carbide in literature [20-21]. This gives the measurement errors in present work of 1.36 % for γ, 2.05% for α and 0.8% for κ, respectively. The lattice misfit around κ-α interface is (3.75-2.92)/3.75 = 22.1%, while that around κ-γ interface is (3.75-3.66)/3.75 = 2.40%. According to the previous results, α-matrix in lower Mn steel contains 18% γ phase and 68% α phase [14]. κ-carbides are surrounded by α phase. The latter is embedded in γ phase [14].

Topotaxy might happen when the κ-carbides are very small nanoscale precipitates. This leads to hardening but κ carbides are cut by the lattice dislocations in α crystals and κ-α the interface is coherent. It is seen clearly that κ-carbide in Fig. 1(c) is not in the case. κ will probably not be cut by the lattice dislocations in α crystals. The κ-α interface is incoherent due to large lattice misfit (22.1%). Orowan loops will be formed and cross slip will be enhanced at the κ carbide. The cross slip may be particularly important for activating secondary slip and the associated hardening. Orowan loops will create back stresses leading to further hardening. This causes the accumulation of significant amount of dislocations around the κ-α interface. α is a

soft matrix. κ-carbide is a hard inclusion. The high dislocation density around an interface between high mechanical contrast crystals (α and κ) is favourable for the crack initiation [22]. The large lamellar κ-carbides leave long and planar κ-α interface. The nucleated cracks are easier to propagate along a planar interface due to less energy dissipation than that along a fractal one. Both the high crack nucleation rate and high crack propagation rate around κ-α interface lead to a poor formability of Fe-26Mn-9Al-0.75C steel. κ-γ interface in Fe-34Mn-9Al-0.65C steel, on the contrary, has small lattice misfit. This causes less high dislocation density and low crack nucleation rate. The fine structure in higher Mn steel prevents the nucleated cracks from propagation. This explains why Fe-34Mn-9Al-0.65C steel has better formability. It has been suggested in literature that the alloys with coherent interface (i.e. zero misfit, e.g. twining) possesses ideal mechanical properties [23-24].

Without change chemical composition, the formability of α-matrix-based high Al steel can be improved by two other methods. The first is to modify κ lamellar structure into fine spherical structure in order to prevent crack propagation along planer κ-α interface. The second is to reduce κ volume fraction and hence to retard crack nucleation around κ-α interface. The lattice misfit between κ and α crystals is difficult to change under trivial processing conditions.

3. Electropulsing microstructure to improve the formability

The second objective of the present work was to improve the workability of α-matrix-based high Al steel. According to literature, lamellar structure can be spheroidized [25] and refined [26] by electric current processing (electropulsing). Electropulsing has also been implemented to alternate the volume fraction of precipitate [27-28]. The annealed Fe-26Mn-9Al-0.75C samples were subjected to an electric current pulse with peak current density of 1.92×10^{9} $A\cdot m^{-2}$. The pulse was generated by discharge a capacity at room temperature. The capacitor was charged at 2.5 kv. Pulse is in the damped shape oscillations with initial period around 20 μs and total duration of 110 μs. One pulse was applied to each sample. The microstructure of the electropulsed samples was characterized using the same methods as that described in Section 2. The formability was testified by cold rolling to 70% reduction. The observations were compared to that of the samples without electropulsing treatment.

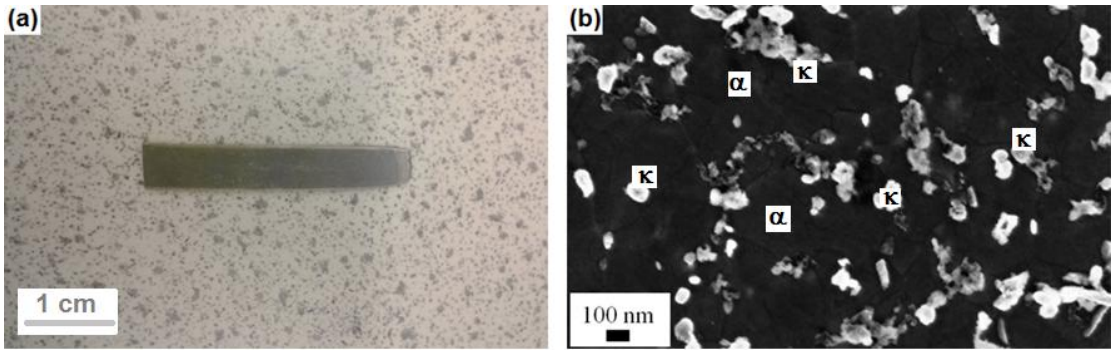


Fig. 2 (a) An electropulsed Fe-26Mn-9Al-0.75C sample after cold rolling to 70% reduction. (b) SEM micrograph shows the spheroidized κ-carbide particle with 250 nm average diameter in an electropulsed Fe-26Mn-9Al-0.75C sample.

Fig. 2(a) shows an electropulsed Fe-26Mn-9Al-0.75C sample after cold rolling to 70% reduction. No cracks were detected from the optical observation. In comparison to those not electropulsed samples, as shown in Fig. 1(a), the formability of electropulsed sample has been improved considerably. To identify the causes of the improvement, the microstructure was analysed by SEM. Fig. 2(b) presents a SEM micrograph of the electropulsed samples. The grey particles in the image are κ-carbides. The previous lamellar κ structure has been converted into sub-micron particulate structure. The average particle size is 250 nm. Image analysis using Image J software reveals that κ volume fraction has been reduced from 14% to 6.8% in the overall sample and from 68% to 31% in some local areas by the electropulsing treatment.

TEM analysis for Fe-26Mn-9Al-0.75C samples before and after electropulsing treatment is presented in Fig. 3. Fig. 3(a) and 3(c) show lamellar κ structure in the samples without electropulsing. Fig. 3(b) and 3(d) show particulate κ structure after electropulsing treatment. The α-matrix structure is also refined significantly. The average α grain size after electropulsing is 1.46 μm. As discussed in Section 2, the spheroidized and refined κ microstructure leads to the improvement of formability. SADP in Fig. 3(e) and the orientation marks in Fig. 3(f) prove that the orientation relationships between κ and α ferrite are unchanged by the electropulsing treatment.

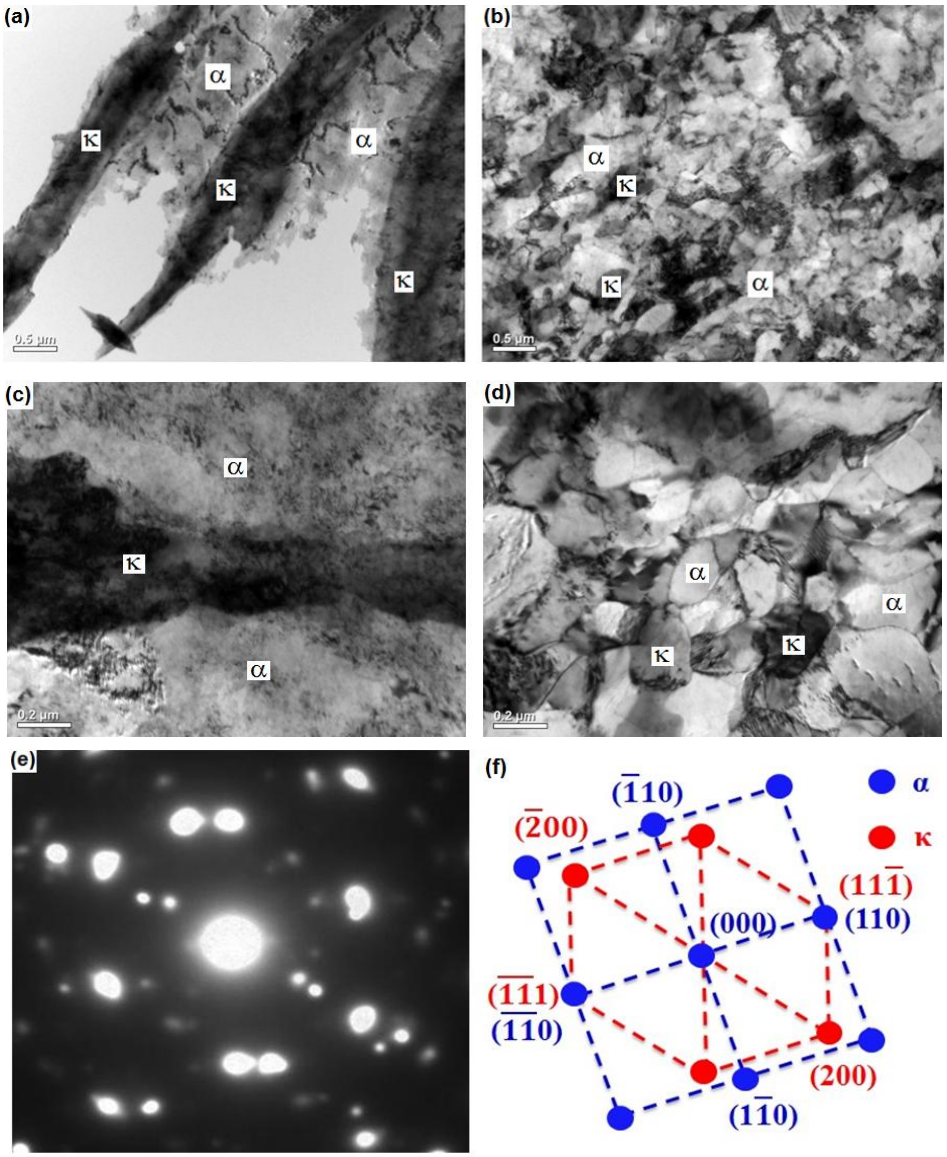


Fig.3 TEM micrographs show the microstructure of the Fe-26Mn-9Al-0.75C samples before ((a) and (c)) and after ((c) and (d)) electropulsing treatment. The selected area diffraction pattern (e) and orientation marks (f) show the unchanged relationships between κ and α crystals after electropulsing treatment.

4. Discussion

The observed electropulsing-induced microstructure refinement and property improvement cannot be explained by simply a thermal effect. Theoretical calculation

predicts the maximum current-induced temperature rising of around 200 ^{o}C [29-30]. The recrystallization temperature for the steel is the range of 450-750 ^{o}C. The temperature rising due to Ohm heat is too low to enable microstructure transformations.

To prove that the observed electropulsing-induced microstructure evolution is not only taken place in some local areas but throughout the sample, electrical conductivity of the sample before and after the electropulsing treatment was measured using DO5000 series Microhmmeter. The measured electrical conductivities before and after electropulsing treatment are 6.37×10^6 S/m and 7.94×10^6 S/m, respectively. It increases 24.6%. Matthiessen's rule states that the total electrical resistivity of an impure metal includes the temperature-dependent intrinsic resistivity ($\rho_0(T)$) arising from the scattering of electrons by lattice waves or phonons and the residual resistivity ($\rho_R(c)$) caused by the scattering of electrons by impurity atoms and lattice defects which is temperature independent but dependent on the impurity concentration (c) [31]. This is represented as [31-32]

$$\rho(c,T) = \rho_0(T) + \rho_R(c) \approx \rho_0(T) + \sum_i c_i \rho_i \quad (1)$$

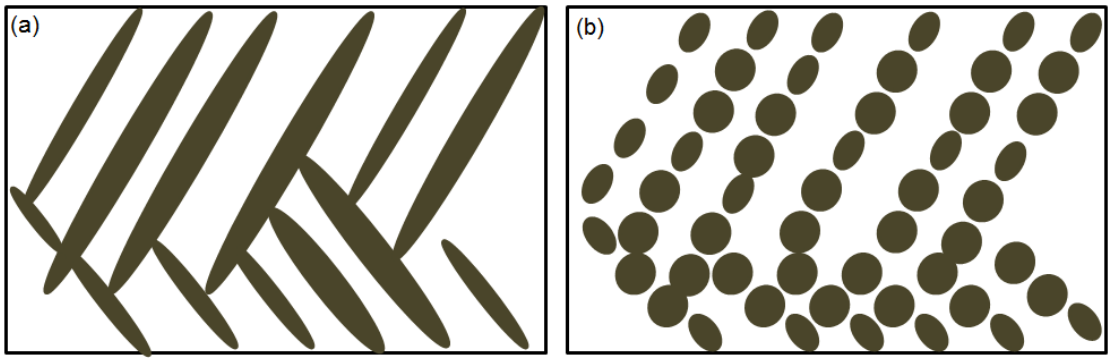


Fig. 4. Schematic diagrams illustrate that the electrical resistivity of a material with microstructure (a) is larger than that of (b) when the grey phase has larger conductivity than that of the matrix. The figure was drawn following the similar concept in literature [30, 33].

where ρ_i is the elemental resistivity of solute *i* in the matrix [32]. For transition metals (e.g. Fe), electron-electron scattering makes a significant contribution to $\rho_0(T)$ at low temperature. It is found that $\rho_0(T)$ should be represented by $1/(1/\rho_0(T)+1/\rho_{sat})$ for steels, where ρ_{sat} is the saturation resistivity [32]. $\rho_0(T)$ and ρ_{sat} take the same values for all carbides and phases in steels. According to Matthiessen's theory, the electrical resistivity of κ-carbide is higher than that of α phase due to higher C, Al and Mn compositions in κ than in α. In microstructure configurations illustrated in Fig. 4, the system electrical resistivity of lamellar structure in Fig. 4(a) is close to value of that for κ-carbide, but that in Fig. 4(b) is close to that of α phase [30, 33]. The experimental measured values are consented to the theoretical analysis.

The observed microstructure evolution from lamellar to spherical can be understood in electroplasticity framework. Electroplasticity means that the strain rate of a metal can be increased by at least three orders of magnitude by the passing electric current [34]. The critical current density for generation of electroplasticity is 10^3 A/m^2 [35]. The applied electric current density in the present work is well-above that of the critical value. The mobility of the dislocations and elements in steels is enhanced by electric-current for at least 3 orders of magnitude and is proportional to the peak current density [36-37]. This promotes the structure transformation by reducing the kinetic barriers and accelerating kinetics [25]. The structure transformation can take place in a temperature which is much lower than its conventional value. The dislocations formed during materials processing and quenching and accumulated around κ-α interface are migrated into lamellar plates at the temperature [26]. This generates significant interfaces inside the original lamellar plates. The lamellar κ breaks into pieces. The current-enhanced mobility of elements also promotes the spheronization of κ pieces. The structure refinement of κ is hence achieved.

Another effect of electric current is to change the free energy sequence between phases. For a system with electric current passing through, the system free energy consists of chemical free energy, interface energy, strain-stress energy and electric current free energy [38-39]. The electric current free energy is different for different phases due to their different electrical conductivities and magnetic permeabilities. This causes the different change of the total free energy for different phases when current is passing through. The original free energy sequence is hence changed due to

the extra electric current free energy. It has been proved that electric current helps to dissolve low conductive phase embedded in a high conductive matrix [27-28, 38]. The observed reduction of κ-carbides is alongside with this prediction. κ-α interface provides the major crack nucleation sites in the steel. The reduction of κ-α volume fraction leads to less crack nucleation sites. The formability is hence improved.

The cold working properties of high Al steels are also quite profoundly affected by the texture and by the grain size [40-41]. Adequate choose of electropulsing processing parameters can tailor steels texture and grain size [42] in some cases. Optimizing the processing parameters to generate ideal cold working properties is with great research interests [9, 43-44].

A low volume fraction of κ-carbides in high Al steel provides less crack nucleation sites. A refined and spheroidized κ structure prevents micro-cracks from propagation. Those two effects make the formability of high Al steel improved. It is worth pointing out that the formability can be affected by many other factors. The chemical constitution, α-γ interface fraction, distribution of dislocations and defects, the ordered $L1_2$, D03 and B2 structures formed in Fe-Al system [45], and other inclusions and intermetallic phase might also affect the formability. Investigation of relationships between electropulsing and those just mentioned microstructures and the ways to improve the materials formability will be studied in future.

5. Summary

a). The formability of high Al lightweight steel is dependent on the microstructure. The γ-matrix-based high Al steel has better formability than that of α-matrix-based steel. The α-matrix-based lightweight steel has high lattice misfit (22.1%) κ-α interface and coarse lamellar structure. Its cold working formability is low. The γ-matrix-based lightweight steel has low lattice misfit (2.70%) κ-γ interface and fine lamellar structure. k-carbide in higher Mn steels is much finer than that in lower Mn steel. This steel shows good formability. The γ-matrix-based lightweight steel can be obtained by adding more austenite stabilizing elements, e.g. Mn, or using suitable thermomechanical processing conditions.

b). The formability of α-matrix-based lightweight steel can be improved by electropulsing treatment. The process converts the coarse lamellar κ structure into fine particulate structure. The volume fraction of κ is reduced after electropulsing treatment. The crack nucleation and propagation is retarded by in the electropulsed α-matrix-based lightweight steel.

c). Electroplasticity promotes the migration of dislocation into lamellar structure. This causes microstructure transformation at a temperature lower than that in conventional recrystalization. Electropulse-enhanced mobility of elements promotes κ spheroidization. The change of electric current free energy makes dissolution of

κ-carbides possible. The formability of α-matrix-based lightweight steel has been improved significantly.

Acknowledgements

The work was financially supported by EPSRC (EP/J011460/2 and EP/L00030X/1), TATA Steel and the Royal Society Newton Advanced Fellowship (NA150320). The authors are grateful to Professor Kenneth C. Mills and Professor Adrian P. Sutton at Imperial College London for fruitful discussions.

References

[1] H. Kim, D.-W. Suh, N. J. Kim, Fe–Al–Mn–C lightweight structural alloys: a review on the microstructures and mechanical properties, *Sci. Technol. Adv. Mater.*, 14 (2013) 014205.

[2] I. Gutierrez-Urrutia, D. Raabe, Influence of Al content and precipitation state on the mechanical behavior of austenitic high-Mn low-density steels, *Scr. Mater.*, 68 (2013) 343–347.

[3] S. Vercammen, B. Blanpain, B. C. De Cooman, P. Wollants, Cold rolling behaviour of an austenitic Fe–30Mn–3Al–3Si TWIP-steel: the importance of deformation twinning, *Acta Mater.*, 52 (2004) 2005–2012.

[4] C. S. Wang, C. N. Hwang, C. G. Chao, T. F. Liu, Phase transitions in an Fe–9Al–30Mn–2.0C alloy, *Scr. Mater.*, 57 (2007) 809–812.

[5] D. G. Morris, M. A. Muñoz-Morris, L. M. Requejo, New iron–aluminium alloy with thermally stable coherent intermetallic nanoprecipitates for enhanced high-temperature creep strength, *Acta Mater.*, 54 (2006) 2335–2341.

[6] W. K. Choo, J. H. Kim, J. C. Yoon, Microstructural change in austenitic Fe-30.0wt%Mn-7.8wt%Al-1.3wt%C initiated by spinodal decomposition and its influence on mechanical properties, *Acta Metall.*, 45 (1997) 4877–4885.

[7] K. M. Chang, C. G. Chao, T. F. Liu, Excellent combination of strength and ductility in an Fe–9Al–28Mn–1.8C alloy, *Scr. Mater.*, 63 (2010) 162–165.

[8] W. J. Lu, X. F. Zhang, R. S. Qin, Structure and properties of κ-carbides in duplex lightweight steels, *Ironmak. Steelmak.*, 42 (2015) 626-631.

[9] D.T. Pierce, J.A. Jimenez, J. Bentley, D. Raabe, C. Oskay, J.E. Wittig, The influence of manganese content on the stacking fault and austenite/epsilon-martensite interfacial energies in Fe-Mn-(Al-Si) steels investigated by experiment and theory, *Acta Mater.*, 68 (2014) 238-253.

[10] W. C. Cheng, C. Y. Cheng, C.W. Hsua, D. E. Laughlin, Phase transformation of the $L1_2$ phase to kappa-carbide after spinodal decomposition and ordering in an Fe–C–Mn–Al austenitic steel, Mater. Sci. Eng. A, 642 (2015) 128–135.

[11] B. Seol, D. Raabe, P. Choi, H.-S. Park, J.-H. Kwak, C.-G. Park, Direct evidence for the formation of ordered carbides in a ferrite-based low-density Fe-Mn-Al-C alloy studied by transmission electron microscopy and atom probe tomography, *Scr. Mater.*, 68 (2013) 348-353.

[12] I. Gutierrez-Urrutia, D. Raabe, Multistage strain hardening through dislocation substructure and twinning in a high strength and ductile weight-reduced Fe-Mn-Al-C steel, *Acta Mater.*, 60 (2012) 5791-5802.

[13] I. Gutierrez-Urrutia, D. Raabe, Dislocation and twin substructure evolution during strain hardening of an Fe–22 wt.% Mn–0.6 wt.% C TWIP steel observed by electron channeling contrast imaging, *Acta Mater.*, 59 (2011) 6449–6462.

[14] W. J. Lu, X. F. Zhang, R. S. Qin, κ -carbide hardening in a low-density high-Al high-Mn, *Mater. Lett.*, 138 (2015) 96–99.

[15] H. Springer, D. Raabe, Rapid alloy prototyping: Compositional and thermo-mechanical high throughput bulk combinatorial design of structural materials based on the example of 30Mn–1.2C–xAl triplex steels, *Acta Mater.* 60 (2012) 4950–4959.

[16] W.-C. Cheng, Y.-S. Song, Y.-S. Lin, K.-F. Chen, P. C. Pistorius, On the eutectoid reaction in a quaternary Fe-C-Mn-Al Alloy: austenite → ferrite + kappa-carbide + $M_{23}C_6$ carbide, *Metall. Mater. Trans. A*, 45(2013) 1199-1216.

[17] I. Gutierrez-Urrutia, D. Raabe, High strength and ductile low density austenitic FeMnAlC steels: Simplex and alloys strengthened by nanoscale ordered carbides, *Mater. Sci. Technol.* 30 (2014) 1099-1104.

[18] D. Raabe, H. Springer, I. Gutierrez-Urrutia, F. Roters, M. Bausch, J.B. Seol, M. Koyama, P.P. Choi, K. Tsuzaki. alloy design, combinatorial synthesis, and microstructure-property relations for low-density Fe-Mn-Al-C austenitic steels, *JOM*, 66 (2014) 1845-1856.

[19] S. Y. Han, S. Y. Shin, S. Lee, N. J. Kim, J.-H. Kwak, K.-G. Chin, Effect of carbon content on cracking phenomenon occurring during cold rolling of three light-weight steel plates, *Metall. Mater. Trans. A*, 42 (2010) 138–146.

[20] M. Onink, C.M. Brakman, F.D. Tichelaar, E.J. Mittemeijer, S. van der Zwaag, J.H. Root, N.B. Konyer, The lattice-parameters of austenite and ferrite in fe-c alloys as functions of carbon concentration and temperature, *Scr. Metall.* Mater., 29 (1993) 1011-1016.

[21] M.Palm, G. Inden, Experimental-determination of phase equilibria in the Fe-Al-C system, *Intermet.*, 3 (1995) 443–454.

[22] I. Gutierrez-Urrutia, D. Raabe, Microbanding mechanism in an Fe-Mn-C high-Mn twinning-induced plasticity steel, *Scr. Mater*., 69 (2013) 53-56.

[23] B. C. De Cooman, O. Kwon, K. G. Chin, State-of-the-knowledge on TWIP steel, *Mater. Sci. Technol*., 28 (2012) 513-527.

[24] K. Lu, L. Lu, S. Suresh, Strengthening materials by engineering coherent internal boundaries at the nanoscale, *Science*, 324 (2009) 349-352.

[25] E. I. Samuel, A. Bhowmik, R. S. Qin, Accelerated spheroidization induced by high intensity electric pulse in a severely deformed eutectoid steel, *J. Mater. Res.*, 25 (2010) 1020-1024.

[26] R. S. Qin, E. I. Samuel, A. Bhowmik, Electropulse-induced cementite nanoparticle formation in deformed pearlitic steels, *J. Mater. Sci.*, 46 (2011) 2838–2842.

[27] Y. B. Jiang, G. Y. Tang, C. H. Shek, Y. H. Zhu, Z. H. Xu, On the thermodynamics and kinetics of electropulsing induced dissolution of b-Mg17Al12 phase in an aged Mg–9Al–1Zn alloy, *Acta Mater.*, 57 (2009) 4797–4808.

[28] W. J. Lu, X. F. Zhang, R. S. Qin, Stability of precipitates under electropulsing in 316L stainless steel, *Mater. Sci. Technol.*, 31 (2015) 1530-1535.

[29] W. J. Lu, X. F. Zhang, R. S. Qin, Electropulsing-induced strengthening of steel at high temperature, *Phil. Mag. Lett.*, 94 (2014) 688–695.

[30] R. S. Qin, A. Rahnama, W. J. Lu, X. F. Zhang, B. Elliott-Bowman, Electropulsed steels, *Mater. Sci. Technol.*, 30 (2014) 1040–1044.

[31] P.D. Desai, H.M. James, C.Y. Ho, Electrical Resistivity of Aluminium and Mananese, *J. Phys. Chem. Ref. Data*, 13 (1984) 1131-1172.

[32] U. Bohnenkamp, R. Sandström, Electrical resistivity of steels and face-centered-cubic iron, *J. Appl. Phys*., 92 (2002) 4402-4407.

[33] A. Rahnama, R.S. Qin, Electropulse-induced microstructural evolution in a ferritic-pearlitic 0.14% C steel, *Scr. Mater.* 96 (2015) 17-20.

[34] H. Conrad, Effects of electric current on solid state phase transformations in metals, *Mater. Sci. Eng. A*, 287 (2010) 227-237.

[35] O. A. Troitskii: 'Electromechanical effect in metals', *JETP Lett.* (English version), 10 (1969) 11–14.

[36] S. H. Xiao, Y. Z. Zhou, J. D. Guo, S. D. Wu, G. Yao, S. X. Li, G. H. He, B. L. Zhou, The effect of high current pulsing on persistent slip bands in fatigued copper single crystals, *Mater. Sci. Eng. A*, 332 (2002) 351-355.

[37] P. S. Ho, T. Kwok: Electromigration in metals, *Rep. Prog. Phys*., 52 (1989) 301–348.

[38] Y. Dolinsky, T. Elperin, Thermodynamics of nucleation in current-carrying conductors, *Phys. Rev. B*, 50 (1994) 52–58.

[39] R.S. Qin, A. Bhowmik, Computational thermodynamics in electric current metallurgy, *Mater. Sci. Technol.*, 31 (2015) 1560-1563.

[40] I. Gutierrez-Urrutia, S. Zaefferer, D. Raabe, The effect of grain size and grain orientation on deformation twinning in a Fe-22 wt.% Mn-0.6 wt.% C TWIP steel, *Mater. Sci. Eng. A* 527 (2010) 3552-3560.

[41] I. Gutierrez-Urrutia, D. Raabe, Grain size effect on strain hardening in twinning-induced plasticity steels, *Scr. Mater.* 66 (2012) 992-996.

[42] J. Kuang, X.H. Li, X.X. Ye, J.G. Tang, H.F. Liu, J. Wang, G.Y. Tang, microstructure and texture evolution of magnesium alloys during electropulse treatment, *Metall. Mater. Trans. A*, 46 (2015) 1789-1804.

[43] J. Kuang, X.H. Li, R.K. Zhang, Y.D. Ye, A. A. Luo, G.Y. Tang, Enhanced rollability of Mg-3Al-1Zn alloy by pulsed electric current: a comparative study, *Mater. Des.* 100 (2016) 204–216.

[44] R.F. Zhu, G.Y. Tang, S.Q. Shi, M.W. Fu, Effect of electroplastic rolling on the ductility and superelasticity of TiNi shape memory alloy, *Mater. Des.*, 44 (2013) 606-611.

[45] R. Oguma, S. Matsumura, T. Eguchi1, Kinetics of B2- and D03-type ordering and formation of domain structures in Fe–Al alloys, *J. Phys.: Condens. Matter.*, 20 (2008) 275225.